Available online at www.sciencedirect.com
ScienceDirect
Journal of Sound and Vibration 320 (2009) 221–234
JOURNAL OF SOUND AND VIBRATION
www.elsevier.com/locate/jsvi

Vibration control of cantilevered Mindlin-type plates

Tao Chen[a,*], Chao Hu[b,c], Wen-Hu Huang[b]

[a]College of Science, Harbin Engineering University, Harbin 150001, China
[b]Department of Aerospace Engineering and Mechanics, Harbin Institute of Technology, Harbin 150001, China
[c]School of Aerospace Engineering and Applied Mechanics, Tongji University, Shanghai 200092, China

Received 1 February 2007; received in revised form 28 May 2008; accepted 17 July 2008
Handling Editor: J. Lam
Available online 5 October 2008

Abstract

The cantilevered structure in aerospace engineering is modeled as plates. Based on the Mindlin's theory of thick plates, the wave/mode control approach is presented to research the active vibration control of the cantilever plate. In the proposed control approach, the independent modal space control and the wave control are designed and applied to suppress vibration. The vibrational behavior of plate systems can be expressed in terms of waves of both propagating and near-field types. A propagating wave incident upon the line discontinuities gives rise to reflected and transmitted waves of both kinds whose amplitudes may be found from the reflection and transmission coefficients. Since the generalized displacement is continuous, considering the equilibrium of the locations of the wave controllers, the wave reflection and transmission coefficients are calculated. The wave controller is designed, and is intended to absorb the vibration energy, especially at higher frequencies. So the flexural vibration of the plate is suppressed. Vibrations of the Mindlin plate per unit disturbance are investigated. The particular controllers considered are the optimal PD/FIR feedback wave controller and modal controller designed using the optimal control approach. At last, numerical results are analyzed and discussed.

1. Introduction

The cantilevered structure is commonly used as elements in the construction of a large number of structures such as spacecraft and large space structures. All these structures have flexible extensions which are made as light and slender as possible due to heavy penalties attached to excessive weight. Such slender elements lack the necessary damping properties of being able to function effectively under dynamic loads. In outer space, solar wind and orbital maneuver may make the plate produce vibration, and the vibration will last for a long time. It will have effect on the normal operation of spacecraft, even its lifetime [1,2]. In order to damp out excessive vibrations and improve the performance of structures, conventional approaches of additional passive damping treatments are not often implemented on these systems because of weights or other constraints. So there has been an increasing interest in active vibration control [3–6]. In active vibration

*Corresponding author. Tel.: +86 451 86419203.
E-mail address: chen_tao1204@163.com (T. Chen).

0022-460X/$ - see front matter
doi:10.1016/j.jsv.2008.07.028

control, desirable performance characteristics are achieved through the application of control forces to a structure.

Vibration can be described in a number of ways, and the most common descriptions are in terms of modes and wave motion. Modal control can suppress vibration of structure through adjusting the feedback gain after state-space equation is established. In the modal approach, the response is described in terms of the undamped modes of vibration of the structure. A finite number of these modes are retained. The control is applied so as to modify the eigenstructure of the system. In modal active vibration control, the aim is to control the characteristics of the modes of vibration, i.e., their damping factors, natural frequencies. There are a number of modal control design methods, two of the most widely used approaches being pole placement and optimal control. However, wave-control approach describes the motion of structure through wave motion equation, and structural vibration is regarded as the waves propagating along different directions. Modal control aims to control the global behavior of the structure, whereas wave control aims to control the flow of vibration energy through the structure. In independent modal space control, the control of the entire infinity of modes requires in principle an infinite number of actuators and sensors, and the higher modes are inevitably uncertain, so complexity and robustness problems may arise, however, wave designs are based on the local properties of the structure, and are inherently much less sensitive to system properties and more robust than global models of structures, especially at higher frequencies. Mei et al. described the wave-control approach, and verified its realizability [7]. The experiment results show that wave control alters the detail of the implementation. For example, in the design of the wave control, near fields were ignored, although these can deteriorate the performance. In a similar way, if the propagating waves are incident from both sides of the control location, then they can interfere and the performance may again deteriorate. The wave controllers that were implemented, however, were guaranteed to be stable. So there are no consequences for closed-loop stability. These problems could be avoided in a number of ways, for example, by implementing wave controllers which sense both displacement and rotation or by the suitable application of two or more wave controllers. Optimal controllers are usually non-causal. This reflects the implicit time delays involved in the propagation of waves from one point in a structure to another. Time-domain implementations are, therefore, causal approximations to the optimums and are usually implemented using causal FIR filters.

In previous investigations, wave control only has been applied to control the wave motion in the one-dimensional waveguides such as bending waves in beams, axial waves in rods, etc. [8–10]. Less frequently, the wave control of plate has been investigated. Pan and Hansen [11] discussed the active vibration control of a semi-infinite plate with one pair of opposite edges simply supported using feedforword control approach. However, cantilevered plate structure is commonly used in aerospace engineering. In a continuous structure, vibrations can alternatively be regarded as being the superposition of waves traveling through the structure. These waves are reflected and transmitted at the structural discontinuities. Active wave control aims to control the distribution of energy in the structure by either reducing the transmission of waves from one part of the structure to another or absorbing the energy carried by the waves. Here the disturbance is detected, and a control force is applied somewhere downstream to cancel the incoming wave or to absorb the energy associated with it.

At present, in vibration control of the structure, it is seldom modeled as Mindlin plates. Although Kusculuoglu and Royston [12] investigated vibration control of Mindlin plates, the wave control of Mindlin plate has not been investigated. In Mindlin's plate theory, the effects of transverse shear and rotary inertia are considered, and the deficiencies of the classical thin plate theory are made up. Therefore, when Mindlin's theory of thick plates is applied to analyze the vibration problem, the result will be more close to the practical situation in engineering. In this paper, based on Mindlin's theory of thick plates, wave/mode control approach is presented to research active vibration control of a cantilever plate. Wave/mode control strategy of structural vibration is analyzed and investigated. Control force/sensor feedback wave control and independent modal space control are considered.

2. Wave motion equations of Mindlin plate and its solution

The structural model of a cantilever plate is considered, as depicted in Fig. 1. According to the Mindlin's plate theory, in the orthogonal coordinates, the displacement components at any point in the vibrating plate

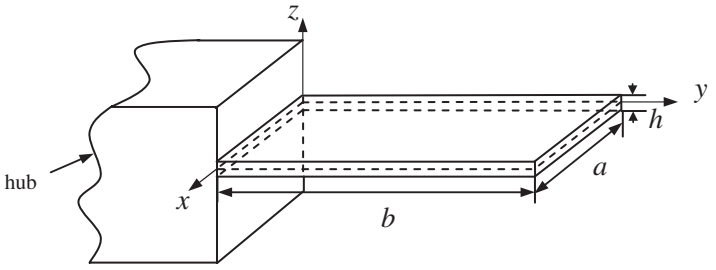

Fig. 1. Modeling of the rectangular plate.

are denoted as u_x, u_y, and u_z. They can be expressed as [13]

$$u_x = z\psi_x(x,y,t), \quad u_y = z\psi_y(x,y,t), \quad u_z = w(x,y,t), \tag{1}$$

where w is the lateral displacement of plates, the quantities ψ_x and ψ_y are, respectively, the cross-sectional rotations in the x and y directions of the deformed median surface. The expressions of bending moment, torsional moment and shearing force in plates are written as

$$M_x = D\left(\frac{\partial\psi_x}{\partial x} + v\frac{\partial\psi_y}{\partial y}\right), \quad M_y = D\left(\frac{\partial\psi_y}{\partial y} + v\frac{\partial\psi_x}{\partial x}\right), \quad M_{xy} = M_{yx} = \frac{(1-v)}{2}D\left(\frac{\partial\psi_y}{\partial x} + \frac{\partial\psi_x}{\partial y}\right), \tag{2a}$$

$$Q_x = C\left(\frac{\partial w}{\partial x} + \psi_x\right), \quad Q_y = C\left(\frac{\partial w}{\partial y} + \psi_y\right), \tag{2b}$$

where D is the bending stiffness of plates, $D = Eh^3/12(1-v^2)$, $C = \kappa Gh$, h the height of the plate, κ is the shearing coefficient with $\kappa = \pi^2/12$, G the shear modulus, and v the Poisson ratio.

According to the equilibrium of torque and force in the cantilever plate, the following can be obtained:

$$\frac{\partial M_x}{\partial x} + \frac{\partial M_{yx}}{\partial y} - Q_x = \rho I\frac{\partial^2\psi_x}{\partial t^2}, \tag{3a}$$

$$\frac{\partial M_{xy}}{\partial x} + \frac{\partial M_y}{\partial y} - Q_y = \rho I\frac{\partial^2\psi_y}{\partial t^2}, \tag{3b}$$

$$\frac{\partial Q_x}{\partial x} + \frac{\partial Q_y}{\partial y} + p = \rho h\frac{\partial^2 w}{\partial t^2}, \tag{3c}$$

where ρ is the mass density of the plate, p the external disturbance, and I the area moment of inertia with $I = h^3/12$.

Substituting Eq. (2) into Eq. (3), the coupled differential equations for vibration of a Mindlin's plate can be obtained:

$$D\left[\frac{\partial^2\psi_x}{\partial x^2} + \frac{(1-v)}{2}\frac{\partial^2\psi_x}{\partial y^2} + \frac{(1+v)}{2}\frac{\partial^2\psi_y}{\partial x\,\partial y}\right] - C\left(\frac{\partial w}{\partial x} + \psi_x\right) = \rho I\frac{\partial^2\psi_x}{\partial t^2}, \tag{4a}$$

$$D\left[\frac{\partial^2\psi_y}{\partial y^2} + \frac{(1-v)}{2}\frac{\partial^2\psi_y}{\partial x^2} + \frac{(1+v)}{2}\frac{\partial^2\psi_x}{\partial x\,\partial y}\right] - C\left(\frac{\partial w}{\partial y} + \psi_y\right) = \rho I\frac{\partial^2\psi_y}{\partial t^2}, \tag{4b}$$

$$C\left(\frac{\partial^2 w}{\partial x^2} + \frac{\partial^2 w}{\partial y^2} + \frac{\partial\psi_x}{\partial x} + \frac{\partial\psi_y}{\partial y}\right) = \rho h\frac{\partial^2 w}{\partial t^2} - p. \tag{4c}$$

Eq. (4) can be depicted by the matrix form, namely,

$$\mathbf{M}\frac{\partial^2\boldsymbol{\xi}}{\partial t^2}-\mathbf{K}\boldsymbol{\xi}=\mathbf{f}, \tag{5}$$

where,

$$\mathbf{M}=\begin{bmatrix}\rho I & 0 & 0\\ 0 & \rho I & 0\\ 0 & 0 & \rho h\end{bmatrix},\quad \mathbf{K}=\begin{bmatrix} D\frac{\partial^2}{\partial x^2}+\frac{1-v}{2}D\frac{\partial^2}{\partial y^2}-C & \frac{1+v}{2}D\frac{\partial^2}{\partial x\,\partial y} & -C\frac{\partial}{\partial x}\\ \frac{1+v}{2}D\frac{\partial^2}{\partial x\,\partial y} & D\frac{\partial^2}{\partial y^2}+\frac{1-v}{2}D\frac{\partial^2}{\partial x^2}-C & -C\frac{\partial}{\partial y}\\ -C\frac{\partial}{\partial x} & -C\frac{\partial}{\partial y} & 0\end{bmatrix},$$

$$\boldsymbol{\xi}=\begin{bmatrix}\psi_x & \psi_y & w\end{bmatrix}^{\mathrm{T}},\quad \mathbf{f}=[0\quad 0\quad p]^{\mathrm{T}}.$$

The displacement can be discretized such that

$$\boldsymbol{\xi}(x,y,t)=\sum_{i=1}^{\infty}\sum_{j=1}^{\infty}\boldsymbol{\xi}_{i,j}(x,y)q_{i,j}(t), \tag{6}$$

where $\boldsymbol{\xi}_{i,j}(x,y)=\begin{bmatrix}\Psi_{xi,xj}(x,y) & \Psi_{yi,yj}(x,y) & W_{i,j}(x,y)\end{bmatrix}^{\mathrm{T}}$, and $q_{i,j}(t)$ denotes the modal coordinates.

Substituting Eq. (6) into Eq. (5), one obtains

$$\mathbf{M}\sum_{i=1}^{\infty}\sum_{j=1}^{\infty}\boldsymbol{\xi}_{i,j}\frac{\partial^2 q_{i,j}}{\partial t^2}-\mathbf{K}\sum_{i=1}^{\infty}\sum_{j=1}^{\infty}\boldsymbol{\xi}_{i,j}q_{i,j}=\mathbf{f}, \tag{7}$$

where $\boldsymbol{\xi}_{i,j}(x,y)$ is the mode shape and it should satisfy the following homogeneous differential equation:

$$\mathbf{M}\boldsymbol{\xi}_{i,j}\omega_{i,j}^2+\mathbf{K}\boldsymbol{\xi}_{i,j}=\mathbf{0}. \tag{8}$$

Substituting Eq. (8) into Eq. (7), one obtains

$$\sum_{i=1}^{\infty}\sum_{j=1}^{\infty}\mathbf{M}\boldsymbol{\xi}_{i,j}\frac{\partial^2 q_{i,j}}{\partial t^2}+\sum_{i=1}^{\infty}\sum_{j=1}^{\infty}\mathbf{M}\omega_{i,j}^2\boldsymbol{\xi}_{i,j}q_{i,j}=\mathbf{f}. \tag{9}$$

The equation of motion can then be written in terms of the modal coordinates by multiplying by $\boldsymbol{\xi}_{r,s}(x,y)$ and integrating over the plate structure, namely,

$$\iint_{\Omega}\sum_{i=1}^{\infty}\sum_{j=1}^{\infty}\boldsymbol{\xi}_{r,s}^{\mathrm{T}}\mathbf{M}\boldsymbol{\xi}_{i,j}\frac{\partial^2 q_{i,j}}{\partial t^2}\,\mathrm{d}x\,\mathrm{d}y+\iint_{\Omega}\sum_{i=1}^{\infty}\sum_{j=1}^{\infty}\omega_{i,j}^2\boldsymbol{\xi}_{r,s}^{\mathrm{T}}\mathbf{M}\boldsymbol{\xi}_{i,j}q_{i,j}\,\mathrm{d}x\,\mathrm{d}y=\iint_{\Omega}\boldsymbol{\xi}_{r,s}^{\mathrm{T}}\mathbf{f}(x,y,t)\,\mathrm{d}x\,\mathrm{d}y. \tag{10}$$

Here the mode shapes are assumed to be normalized such that

$$\iint_{\Omega}\boldsymbol{\xi}_{r,s}^{\mathrm{T}}\mathbf{M}\boldsymbol{\xi}_{i,j}\,\mathrm{d}x\,\mathrm{d}y=\delta_{i,r}\delta_{j,s},\quad i,j,r,s=1,2,\ldots. \tag{11}$$

So, we have

$$\frac{\partial^2 q_{i,j}(t)}{\partial t^2}+\omega_{i,j}^2 q_{i,j}(t)=\mathbf{f}_{r,s}(t),\quad f_{r,s}(x,y,t)=\iint_{\Omega}\boldsymbol{\xi}_{r,s}^{\mathrm{T}}f(x,y,t)\,\mathrm{d}x\,\mathrm{d}y. \tag{12}$$

The spatial variations $W(x,y)$, $\Psi_x(x,y)$, and $\Psi_y(x,y)$ are expressed as a series of products of the x- and y-functions. The variations of $W(x,y)$ and $\Psi_x(x,y)$ along the x direction and of $W(x,y)$ and $\Psi_y(x,y)$ along the y direction can be directly related to appropriate Timoshenko beam functions. On the other hand, the variation of $\Psi_x(x,y)$ along y and the variation of $\Psi_y(x,y)$ along x cannot, at first sight, be directly related to

any beam function. A way out of this difficulty was provided by studying the eigenvectors of finite strip solutions of Mindlin plate vibration for a rectangular plate [14]. The variation of $\Psi_x(x, y)$ along y is of a shape very similar to that of the variation of $W(x, y)$ along y and similarly $\Psi_y(x, y)$ and $W(x, y)$ are of a shape very similar along x. Sets of beam displacement functions are assumed in the free–free and clamped–free directions of a rectangular plate, with products of these functions giving the assumed displacement at any point on the plate. So the spatial variations of the three fundamental quantities are taken to be of the following forms [15]:

$$w(x,y,t) = \sum_{i=1}^{\infty}\sum_{j=1}^{\infty} a_{ij} w_i(x) w_j(y) q_{i,j}(t), \tag{13a}$$

$$\psi_x(x,y,t) = \sum_{i=1}^{\infty}\sum_{j=1}^{\infty} b_{ij} \varphi_i(x) w_j(y) q_{i,j}(t), \tag{13b}$$

$$\psi_y(x,y,t) = \sum_{i=1}^{\infty}\sum_{j=1}^{\infty} c_{ij} w_i(x) \varphi_j(y) q_{i,j}(t), \tag{13c}$$

where $w_i(x)$ and $\varphi_i(x)$ are assumed to be free–free Timoshenko beam modes along the x direction, and $w_j(y)$ and $\varphi_j(y)$ are assumed to be clamped–free Timoshenko beam modes along the y direction. a_{ij}, b_{ij}, and c_{ij} can be determined by Ritz method, and hence yield the natural frequencies and mode shapes [16].

So, based on Timoshenko beam theory, the ith mode shape of general displacement along x direction can be expressed as [17]

$$w_i(x) = a_1 \cos(k_{11}x) + a_2 \sin(k_{11}x) + a_3 \cos(k_{12}x) + a_4 \sin(k_{12}x), \tag{14a}$$

$$\varphi_i(x) = d_1 \cos(k_{11}x) + d_2 \sin(k_{11}x) + d_3 \cos(k_{12}x) + d_4 \sin(k_{12}x), \tag{14b}$$

where k_{11} and k_{12} are the wave numbers of propagating waves and near-field waves along the x direction, respectively. a_i and d_i determined by satisfying the boundary condition are the mode coefficients, respectively. a_i and d_i are given in the appendix.

Following the work of Carvalho [5], we obtain

$$k_{11,12}^2 = \frac{1}{2}\left\{k_0^4 \frac{h^2}{12}\left[1 + \frac{24(1+\nu)}{\pi^2} \pm \sqrt{\Delta}\right]\right\}, \tag{15}$$

where $\Delta = \{k_0^4(h^2/12)[1 + 24(1+\nu)/\pi^2]\}^2 - 4k_0^4[k_0^4 h^4(1+\nu)/6\pi^2 - 1]$ and $k_0 = (\rho h\omega^2/D)^{1/4}$ is the wave number of elastic waves.

Equation satisfying the boundary conditions of beam is given by

$$\begin{aligned}&\left[\left(k_{11}^2 - \frac{\rho h\omega^2}{C}\right)^2 k_{11}^2 + \left(k_{12}^2 - \frac{\rho h\omega^2}{C}\right)^2 k_{12}^2\right]\sin(k_{11}a)\sin(k_{12}a) + 2k_{11}k_{12}\left(\frac{\rho h\omega^2}{C} - k_{12}^2\right)\\ &\times\left(\frac{\rho h\omega^2}{C} - k_{11}^2\right)\cos(k_{11}a)\cos(k_{12}a) + 2k_{11}k_{12}\left(\frac{\rho h\omega^2}{C} - k_{12}^2\right)\left(k_{11}^2 - \frac{\rho h\omega^2}{C}\right) = 0.\end{aligned} \tag{16}$$

Similarly, the jth mode shape of the general displacement along the y direction can be expressed as

$$w_j(y) = b_1 \cos(k_{21}y) + b_2 \sin(k_{21}y) + b_3 \cos(k_{22}y) + b_4 \sin(k_{22}y), \tag{17a}$$

$$\varphi_j(y) = c_1 \cos(k_{21}y) + c_2 \sin(k_{21}y) + c_3 \cos(k_{22}y) + c_4 \sin(k_{22}y), \tag{17b}$$

where k_{21} and k_{22} are wave numbers of propagating waves and near-field waves along y direction, respectively. b_i and c_i determined satisfying the boundary condition are the respective mode coefficients b_i and c_i are given in the appendix.

Considering the cantilever beam, equation satisfying the boundary conditions of beam is given by

$$\left[\left(k_{21}^2-\frac{\rho h}{C}\omega^2\right)^2+\left(k_{22}^2-\frac{\rho h}{C}\omega^2\right)^2\right]k_{21}k_{22}\cos(k_{21}b)\cos(k_{22}b)$$
$$+(k_{21}^2+k_{22}^2)\left[k_{21}^2-\frac{\rho h}{C}\omega^2\right]\left[k_{22}^2-\frac{\rho h}{C}\omega^2\right]\sin(k_{21}b)\sin(k_{22}b)$$
$$-2k_{21}k_{22}\left(k_{21}^2-\frac{\rho h}{C}\omega^2\right)\left(k_{22}^2-\frac{\rho h}{C}\omega^2\right)=0. \tag{18}$$

The maximum kinetic energy of the vibrating plate is expressed as

$$T_{\max}=\frac{1}{2}\iint_{\Omega}[\rho h W^2+\rho I(\psi_x^2+\psi_x^2)]\mathrm{d}x\,\mathrm{d}y, \tag{19}$$

The maximum stain energy of the vibrating Mindlin plate is written as

$$\Pi=\frac{1}{4}\iint_{\Omega}\{D(1+v)(\Gamma_x+\Gamma_y)^2+2C(\Gamma_{yz}^2+\Gamma_{xz}^2)+D(1-v)[(\Gamma_x-\Gamma_y)^2+\Gamma_{yx}^2]\}\mathrm{d}x\,\mathrm{d}y, \tag{20}$$

where $\Gamma_x=\partial\psi_x/\partial x$, $\Gamma_y=\partial\psi_y/\partial y$, $\Gamma_{yx}=\partial\psi_y/\partial x+\partial\psi_x/\partial y$, $\Gamma_{xz}=\psi_x+\partial w/\partial x$, and $\Gamma_{yz}=\psi_y+\partial w/\partial y$.

According to the variational principle, the natural frequencies of the plate are expressed as

$$\omega^2=\Pi/T_{\max}. \tag{21}$$

Upon introducing the state vector $x_{i,j}(t)=[q_{i,j}(t),\dot{q}_{i,j}(t)]^{\mathrm{T}}$, Eq. (12) is rewritten in state-space form as

$$\dot{x}_{i,j}(t)=\bar{A}_{i,j}x_{i,j}(t)+\bar{B}_{i,j}f_{i,j}(t). \tag{22}$$

Here

$$\bar{A}_{i,j}=\begin{bmatrix}0 & 1\\ -\omega_{i,j}^2 & 0\end{bmatrix}\quad \bar{B}_{i,j}=\begin{bmatrix}0\\ 1\end{bmatrix}. \tag{23}$$

3. Independent modal space control

Independent modal space control is now implemented by applying state-space control to the noncontrolled structure. The optimal control design approach is used. The performance index of each mode is represented as

$$J_{i,j}=\int_0^{\infty}(x_{i,j}^{\mathrm{T}}Q_{i,j}x_{i,j}+f_{i,j}^{\mathrm{T}}R_{i,j}f_{i,j})\,\mathrm{d}t, \tag{24}$$

where $Q_{i,j}$ and $R_{i,j}$ are positive semidefinite and positive weighting matrices. The ith modal control force may be written as

$$f_{i,j}=-R_{i,j}^{-1}\bar{B}_{i,j}^{\mathrm{T}}P_{i,j}x_{i,j}, \tag{25}$$

where the Riccati gain matrix $P_{i,j}$ is the solution to the algebraic Riccati equation.

$$-P_{i,j}\bar{A}_{i,j}-\bar{A}_{i,j}^{\mathrm{T}}P_{i,j}-Q_{i,j}+P_{i,j}\bar{B}_{i,j}R_{i,j}^{-1}\bar{B}_{i,j}^{\mathrm{T}}P_{i,j}=0. \tag{26}$$

4. Feedback wave control

4.1. Wave transmission and reflection at the line discontinuities

Vibrations can be regarded as the superstition of the waves traveling through the structure. Wave controllers may be applied at the line parallel to the x direction where the structure is uniform. The point

discontinuities on the beam now become the line discontinuities [18]. In this paper, collocated force/sensor negative feedback control is assumed to be applied. In the frequency domain, the wave-control force is given by

$$F(\omega) = -H_w(\omega)w(\omega), \tag{27}$$

where $H_w(\omega)$ is the transfer function of the controller. Note that the amplitudes of any incident near fields are neglected.

A set of positive-going propagating waves are incident on the control location along y and gives rise to the reflected and transmitted waves, as shown in Fig. 2. Consider a plate lying in the $x-y$ plane. Line discontinuities are parallel to the x direction. Wave control is applied at the position of $y = 0$. The generalized displacements $\xi_-(x, y)$ and $\xi_+(x, y)$ of the plate in the regions $y \leqslant 0$ and $y \geqslant 0$ are given by

$$\xi_-(x,y) = \begin{bmatrix} w_- \\ \psi_{x-} \\ \psi_{y-} \end{bmatrix} = \begin{bmatrix} a^+ \\ b^+ \\ c^+ \end{bmatrix} X(x)\exp(\mathrm{i}k_{21}y) + \begin{bmatrix} a^- \\ b^- \\ c^- \end{bmatrix} X(x)\exp(-\mathrm{i}k_{21}y) + \begin{bmatrix} a_N^- \\ b_N^- \\ c_N^- \end{bmatrix} X(x)\exp(k_{22}y), \tag{28a}$$

$$\xi_+(x,y) = \begin{bmatrix} w_+ \\ \psi_{x+} \\ \psi_{y+} \end{bmatrix} = \begin{bmatrix} d^+ \\ e^+ \\ f^+ \end{bmatrix} X(x)\exp(\mathrm{i}k_{21}y) + \begin{bmatrix} d_N^+ \\ e_N^+ \\ f_N^+ \end{bmatrix} X(x)\exp(-k_{22}y), \tag{28b}$$

where the time dependence $\exp(\mathrm{i}\omega t)$ has been suppressed. The terms $\exp(\mathrm{i}k_{21}y)$ and $\exp(-\mathrm{i}k_{21}y)$ represent the propagating and energy-carrying waves, whereas $\exp(-k_{22}y)$ and $\exp(k_{22}y)$ represent near-field waves carrying no energy. The aim of the wave control is to absorb the energy associated with the propagating waves.

Since the plate is continuous, furthermore, by considering the equilibrium at the position of $y = 0$, one has

$$w_+(x,0) = w_-(x,0), \tag{29a}$$

$$\psi_{x+}(x,0) = \psi_{x-}(x,0), \tag{29b}$$

$$\psi_{y-}(x,0) = \psi_{y+}(x,0), \tag{29c}$$

$$M_{y+}(x,0) = M_{y-}(x,0), \tag{29d}$$

$$M_{yx+}(x,0) = M_{yx-}(x,0), \tag{29e}$$

$$Q_{y+}(x,0) - Q_{y-}(x,0) = Hw_+, \tag{29f}$$

where sign $-$ and $+$ denote the corresponding mechanical quantity in the regions $y \leqslant 0$ and $y \geqslant 0$, respectively.

From Eqs. (2b), (29c), and (29f), the following can be obtained:

$$\frac{\partial w_+(x,0)}{\partial y} - \frac{\partial w_-(x,0)}{\partial y} = \frac{Hw_+(x,0)}{C}. \tag{30a}$$

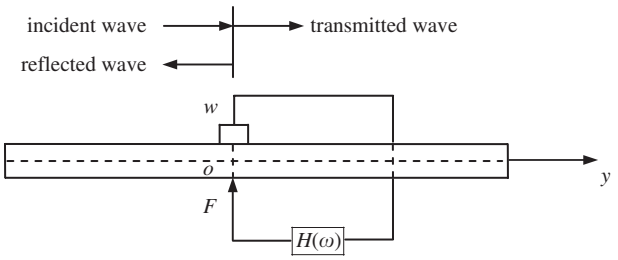

Fig. 2. Schematic diagram of feedback control.

From Eqs. (2a), (4c), (29b), and (29d), the following can be obtained:

$$\frac{\partial^2 w_+(x,0)}{\partial y^2} - \frac{\partial^2 w_-(x,0)}{\partial y^2} = 0. \tag{30b}$$

When the time harmonic loading is imposed, one obtains

$$\frac{\partial^3 w_+(x,0)}{\partial y^3} - \frac{\partial^3 w_-(x,0)}{\partial y^3} = \frac{H w_+ \rho h \omega^2}{C^2}. \tag{30c}$$

Substituting Eq. (28) into Eq. (30) gives

$$\begin{bmatrix} 1 \\ \mathrm{i}k_{21} \end{bmatrix} a^+ + \begin{bmatrix} 1 & 1 \\ -\mathrm{i}k_{21} & k_{22} \end{bmatrix} A^- = \begin{bmatrix} 1 & 1 \\ \mathrm{i}k_{21} - H/C & -k_{22} - H/C \end{bmatrix} D^+, \tag{31a}$$

$$\begin{bmatrix} k_{21}^2 \\ \mathrm{i}k_{21}^3 \end{bmatrix} a^+ + \begin{bmatrix} k_{21}^2 & -k_{22}^2 \\ -\mathrm{i}k_{21}^3 & -k_{22}^3 \end{bmatrix} A^- = \begin{bmatrix} k_{21}^2 & -k_{22}^2 \\ \mathrm{i}k_{21}^3 + H\rho h\omega^2/C^2 & k_{22}^3 + H\rho h\omega^2/C^2 \end{bmatrix} D^+, \tag{31b}$$

Here,

$$D^+ = \begin{bmatrix} d^+ \\ d_N^+ \end{bmatrix} = \begin{bmatrix} t_1 \\ t_2 \end{bmatrix} a^+, \quad A^- = \begin{bmatrix} a^- \\ a_N^- \end{bmatrix} = \begin{bmatrix} r_1 \\ r_2 \end{bmatrix} a^+, \tag{32}$$

where t_1 and t_2 are the transmission coefficients, r_1 and r_2 are the reflection coefficients.

Substituting Eq. (32) into Eq. (31), and letting $\bar{H} = H/Ck_{21}$, $\rho h\omega^2/C = 2h^2k_0^4/(1-v)\pi^2$, one obtains

$$1 + r_1 + r_2 = t_1 + t_2, \quad \mathrm{i} - \mathrm{i}r_1 + \frac{k_{22}}{k_{21}} r_2 = (\mathrm{i} - \bar{H})t_1 - \left(\frac{k_{22}}{k_{21}} + \bar{H}\right) t_2, \tag{33a}$$

$$1 + r_1 - \frac{k_{22}^2}{k_{21}^2} r_2 = t_1 - \frac{k_{22}^2}{k_{21}^2} t_2, \quad \mathrm{i} - \mathrm{i}r_1 - \frac{k_{22}^3}{k_{21}^3} r_2 = \left(\frac{2\bar{H}h^2k_0^4}{(1-v)\pi^2k_{21}^2} + \mathrm{i}\right) t_1 + \left(\frac{2\bar{H}h^2k_0^4}{(1-v)\pi^2k_{21}^2} + \frac{k_{22}^3}{k_{21}^3}\right) t_2. \tag{33b}$$

So the reflection and transmission coefficients can be expressed as

$$\begin{aligned} r_1 = {} & (g\pi^2k_{22}^3\omega - gv\pi^2k_{22}^3\omega - 2gh^2k_{22}k_0^4\omega)\mathrm{i}/\{(k_{21} - k_{22}\mathrm{i})(\pi^2(-1+v)(gk_{21}^2\omega \\ & + k_{22}^2(1 + \mathrm{i} - g\omega) + k_{21}k_{22}(1 - \mathrm{i} + \mathrm{i}g\omega)) - 2gh^2k_0^4\omega\}, \end{aligned} \tag{34}$$

$$\begin{aligned} t_1 = {} & \{\pi^2(-1+v)((1-\mathrm{i})(k_{21}^2k_{22} + k_{22}^3) + gk_{21}^3\omega) - 2gh^2k_{21}\omega k_0^4\}/\{(k_{21} - k_{22}\mathrm{i}) \\ & \times(\pi^2(-1+v)(gk_{21}^2\omega + k_{22}^2(1 + \mathrm{i} - g\omega) + k_{21}k_{22}(1 - \mathrm{i} + \mathrm{i}g\omega)) - 2gh^2k_0^4\omega\}. \end{aligned} \tag{35}$$

In this paper, the controller is designed to absorb incident vibrational energy by adding optimal damping to the structure. Supposing $\bar{H}(\omega) = (1 + \mathrm{i})\omega g$, the power carried in a propagating wave is proportional to the square of the wave amplitude. Thus the power reflected and transmitted per unit incident power is $P(g) = |r_1|^2 + |t_1|^2$. If the support dissipates no energy at discontinuities, namely, $\bar{H}(\omega)$ is real, the power reflected and transmitted per unit incident power is $P(g) = |r_1|^2 + |t_1|^2 = 1$. In this case, the performance index of optimal control is to make the dissipated energy at discontinuities the maximum. In other words, the optimal control gain g can be found by assuming that a wave is incident on onside of the control location and then by designing the control gain so as to maximize the absorb incoming energy, namely to minimize $|r_1|^2 + |t_1|^2$.

So the power reflected and transmitted per unit incident power is given by

$$P(g) = \{(k_{21}^2 + k_{22}^2)(\pi^4(v-1)^2(2gk_{21}^3k_{22}\omega + g^2k_{21}^4\omega^2 + k_{21}^2k_{22}^2(2-g^2\omega^2) + k_{22}^4(2+g^2\omega^2)) - 4gh^2\pi^2(-1+v)\omega(k_{21}k_{22} + gk_{21}^2\omega^2 - gk_{22}^2\omega^2)k_0^4 + 4g^2h^4\omega^2k_0^8)\}/\{\pi^4(2(1+v^2)k_{21}^4k_{22}^2 + 2g(v-1)^2k_{21}^5k_{22}\omega + 2g(v-1)^2k_{21}^3k_{22}^3\omega + g^2(v-1)^2k_{21}^6\omega^2 + 2(v-1)k_{21}^2k_{22}^4(-2+g\omega + gv\omega) + (v-1)^2k_{22}^6(2-2g\omega+g^2\omega^2)) - 4gh^2\pi^2\omega((v-1)(k_{21}^3k_{22} + k_{21}k_{22}^3 + gk_{21}^4\omega - k_{22}^4(g\omega-1))k_0^4 - (1+v)k_{21}^2k_{22}^2) + 4g^2h^4(k_{21}^2+k_{22}^2)\omega^2k_0^8\}. \tag{36}$$

Then the frequency response of the optimal controller is given by

$$\bar{H}_o(\omega) = (1+\mathrm{i})\omega g. \tag{37}$$

4.2. Controller design

The optimal controller of Eq. (37) is non-causal. Hence, a real-time implementation must be some approximations to this ideal, and here two approaches are described. In the first, proportional-plus-derivative (PD) feedback control is implemented, with the controller tuned so that it is equal to the optimal controller at some specific frequencies ω_d. The controller then has the frequency response

$$H_w(\omega) = c_1 + c_2(\mathrm{i}\omega), \tag{38}$$

where $c_1 = \omega_d g$ and $c_2 = g$. In the second approach, FIR controller is implemented. A causal approximation can be found by fitting a causal FIR filter to the optimum controller in the least square sense in the frequency domain. The real and imaginary parts are approximated separately over the frequency range using a least squares procedure as [7]

$$\bar{H}_w(\omega) = a + b\omega^2 + \mathrm{i}(c\omega). \tag{39}$$

If the wave forces are applied at $(x_i,\ y_0)$, then the total wave-control force is $p_w(w,x,y,t) = \sum_{i=1}^n p_w(w,t)\delta(x-x_i)\delta(y-y_0)$. For tuned PD control, this becomes

$$p_w(x,y,t) = -[c_1 w(x,y,t) + c_2\dot{w}(x,y,t)]\sum_{i=1}^{n}\delta(x-x_i)\delta(y-y_0). \tag{40}$$

For causal FIR control, the wave-control force is approximated by

$$p_w(x,y,t) = -[aw(x,y,t) - b\ddot{w}(x,y,t) + c\dot{w}(x,y,t)]\sum_{i=1}^{n}\delta(x-x_i)\delta(y-y_0). \tag{41}$$

For collocated wave control, and with the control force approximated by Eq. (40) or (41), the equations of motion can be written in matrix form as

$$\mathbf{M}\ddot{q} + \mathbf{C}\dot{q} + \mathbf{K}q = \mathbf{F}(t), \tag{42}$$

where $\mathbf{F}_i(t) = [f_{1,1}(t) \quad f_{1,2}(t) \quad \cdots \quad f_{n,n}(t)]^{\mathrm{T}}$ and $\mathbf{M}$, $\mathbf{C}$, and $\mathbf{K}$ are the mass, damping, and stiffness matrices, respectively. In the absence of the wave-control force, the mass matrix $\mathbf{M}$ is an $n \times n$ identity matrix, $\mathbf{C}$ is an $n \times n$ zero matrix, and $\mathbf{K}$ is a diagonal matrix of natural frequencies squared.

Upon introducing the state vector $\mathbf{X}(t) = [q^{\mathrm{T}}(t) : \dot{q}^{\mathrm{T}}(t)]^{\mathrm{T}}$, Eq. (42) is rewritten in state-space form as

$$\dot{\mathbf{X}}(t) = \mathbf{A}\mathbf{X}(t) + \mathbf{B}\mathbf{F}(t), \tag{43}$$

where the coefficient matrices are

$$\mathbf{A} = \begin{bmatrix} \mathbf{0} & \boldsymbol{I} \\ -\mathbf{M}^{-1}\mathbf{K} & -\mathbf{M}^{-1}\mathbf{C} \end{bmatrix}, \quad \mathbf{B} = \begin{bmatrix} \mathbf{0} \\ \mathbf{M}^{-1} \end{bmatrix}. \tag{44}$$

5. Numerical examples

In this section, some numerical results will be presented. In what follows, we introduce several dimensionless parameters: the aspect ratio of the plate $a/b = 0.5$, the plate thickness ratio $h/b = 0.1$, Poisson ratio $v = 0.30$ and $\bar{\omega}_i = \omega_i/\omega_1$ ($i = 1,2, \ldots, 9$). The first nine nondimensional natural frequencies are given in Table 1. Modal control is designed to control the first two modes. The optimal control approach is adopted. Let $Q_{i,j} = R_{i,j} = I$, where I is identity matrix.

For simplicity, we only consider a disturbance force and a wave-control force. In Figs. 3 and 5, the unit disturbance force is applied at the position $(x_d, y_d) = (0.50a, 0.15b)$ and the PD wave-control force is applied at $(x_s, y_s) = (0.50a, 0.40b)$. Numerical results show the response at the position $(x_s, y_s) = (0.50a, 0.70b)$. In Figs. 6 and 7, the unit disturbance force is applied at $(x_d, y_d) = (0.50a, 0.25b)$ and the PD wave-control force is applied at $(x_s, y_s) = (0.50a, 0.40b)$. Numerical results show the response at the position $(x_s, y_s) = (0.50a, 0.70b)$. In Fig. 8, the unit disturbance force is applied at $(x_d, y_d) = (0.50a, 0.25b)$ and the PD wave-control force is applied at $(x_s, y_s) = (0.50a, 0.50b)$. Numerical results show the response at the position $(x_s, y_s) = (0.50a, 0.70b)$. In the approximation that tuned PD control (Eq. (22)), the controller is tuned to be optimal at the fourth natural frequency. In Fig. 9, the unit disturbance force is applied at $(x_d, y_d) = (0.50a, 0.25b)$ and the causal FIR wave-control force is applied at $(x_s, y_s) = (0.50a, 0.50b)$. Numerical results show the response at the position $(x_s, y_s) = (0.50a, 0.70b)$. In figures, the value of ordinate is prescribed as common logarithm of the actual deflection.

Figs. 3 and 4 show the frequency responses before and after modal control. The lowest two modes are clearly well controlled, while sharp resonances associated with the uncontrolled modes still exist. Including more modes in the control design can alleviate this problem, but only at the cost of increased model complexity.

Figs. 3 and 5 show that the resonances are sharp before control, while after wave control, controllers add damping to the structure. Energy of structure is absorbed. Sharp resonances (the 4th and 9th mode) are weakened. They also change the natural frequencies somewhat. Since the controller is tuned to be optimal at fourth frequency, relatively good performance can be seen at the fourth frequency. Figs. 3 and 6 show that the frequency responses are different when the disturbance force is applied at different positions.

Table 1
The first nine nondimensional natural frequencies of system

Mode number	1	2	3	4	5	6	7	8	9
Frequency	1.00	1.83	2.13	6.59	7.12	7.16	8.11	8.20	8.35

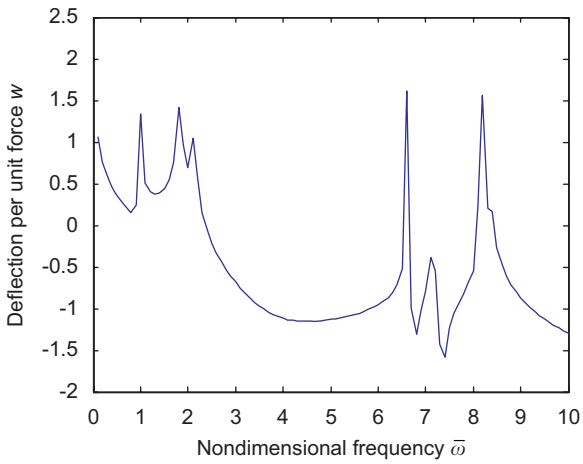

Fig. 3. Frequency response before control.

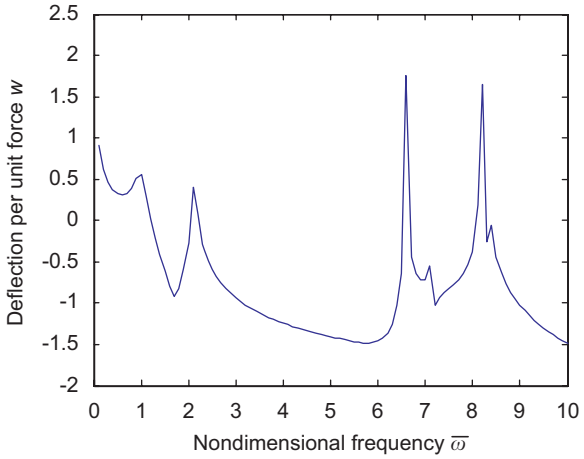

Fig. 4. Frequency response after modal control.

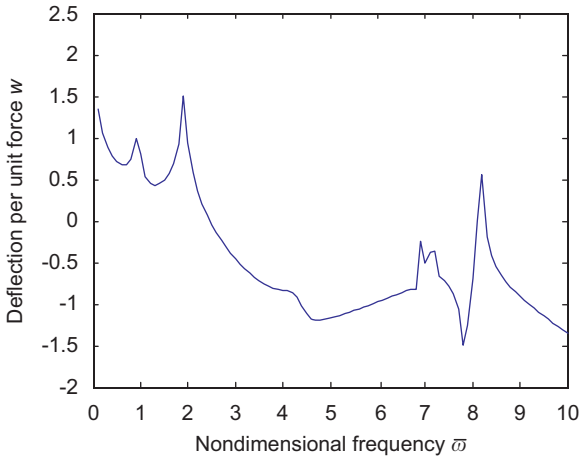

Fig. 5. Frequency response after PD wave control.

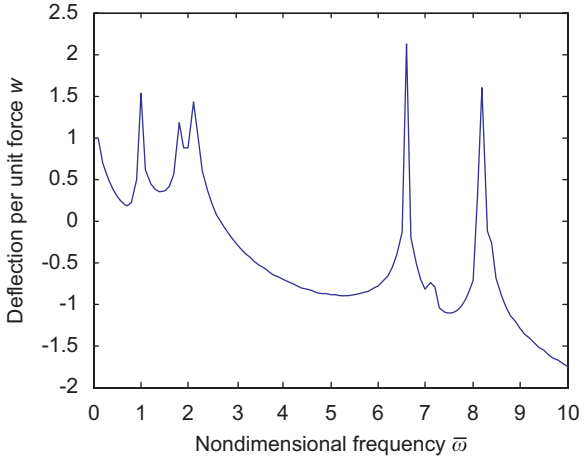

Fig. 6. Frequency response before control.

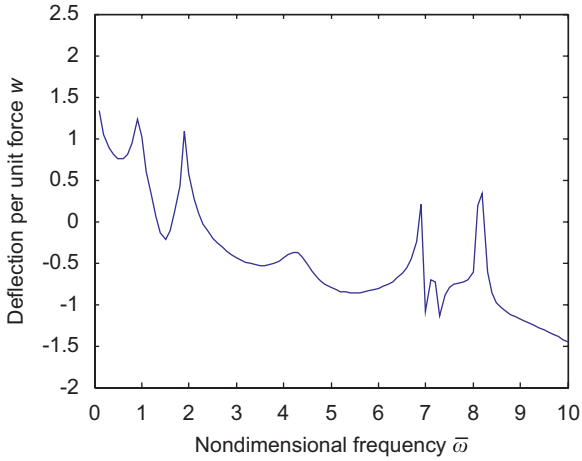

Fig. 7. Frequency response after PD wave control.

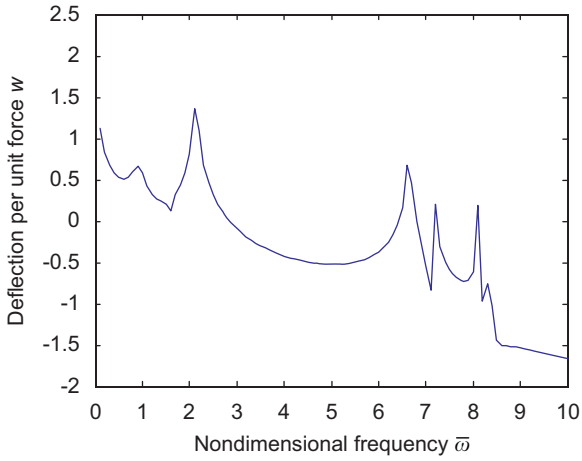

Fig. 8. Frequency response after PD wave control.

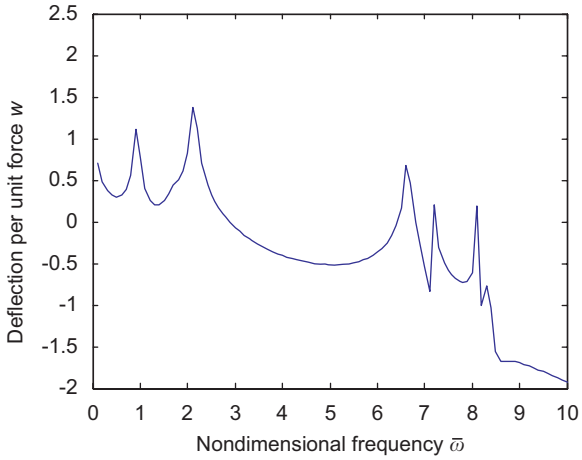

Fig. 9. Frequency response after FIR wave control.

In Figs. 5 and 7, relatively poor performance can also be seen at high frequencies. The degradation of the performance at higher frequencies is due to the fact that the point of application of the wave controller lies close to a node of the 9th mode. Such effects depend on the specific form and location of the wave control. They can be minimized by applying wave control at a boundary, by implementing wave controllers which sense both displacement and rotation or by the suitable application of two or more wave controllers. Figs. 5, 7, and 8 show that the frequency responses have differences when the disturbance force is applied at different positions and wave control force is applied at the same position, or disturbance force is applied at the same position and wave control force is applied at different positions. In Fig. 9, it is seen that the causal FIR control give the same good performance as PD control and relatively poor performance can also be seen at high frequencies.

6. Conclusions

This paper presents the theoretical analysis and numerical results of vibration suppression of Mindlin plate. Wave control is applied to control the wave motion in plates. For simplicity, only flexural waves are considered, because the power carried in longitudinal waves will transfer to more effective radiant flexural wave at structural continuity and discontinuity.

Control gain is designed in frequency domain, and there are many possible approaches to the implementation. Here PD control and causal FIR control are adopted, controller is designed to absorb energy by adding damping to the structure. In the time domain, this corresponds to a tuned spring–damper combination. The PD control gain being calculated is optimal at some desired tuned frequency ω_d. Better performance can be achieved by implementing wave controllers which sense both displacement and rotation or by the suitable application of two or more wave controllers.

Acknowledgment

The paper is supported by the National Natural Science Foundation of China (Foundation no. 10572045) and the Outstanding Youth Foundation of Hei Longjiang Province of China (Foundation no. JC-9).

Appendix

The coefficients satisfying the boundary conditions along x direction are given by

$$a_2=\frac{\left(\frac{\rho h\omega^2}{C}-k_{11}^2\right)\cos(k_{11}a)+\left(k_{11}^2-\frac{\rho h\omega^2}{C}\right)\cos(k_{12}a)}{\left(\frac{\rho h\omega^2}{C}-k_{12}^2\right)\sin(k_{12}a)\frac{k_{12}}{k_{11}}-\left(\frac{\rho h\omega^2}{C}-k_{11}^2\right)\sin(k_{11}a)}a_1,\quad a_3=\frac{\frac{\rho h\omega^2}{C}-k_{11}^2}{k_{12}^2-\frac{\rho h\omega^2}{C}}a_1,\quad a_4=-\frac{k_{12}}{k_{11}}a_2,$$

$$d_1=-\frac{\left(\frac{\rho h\omega^2}{C}-k_{11}^2\right)\left[\left(\frac{\rho h\omega^2}{C}-k_{11}^2\right)\cos(k_{11}a)+\left(k_{11}^2-\frac{\rho h\omega^2}{C}\right)\cos(k_{12}a)\right]}{\left(\frac{\rho h\omega^2}{C}-k_{12}^2\right)\sin(k_{12}a)k_{12}-k_{11}\left(\frac{\rho h\omega^2}{C}-k_{11}^2\right)\sin(k_{11}a)}a_1,\quad d_2=\frac{\frac{\rho h\omega^2}{C}-k_{11}^2}{k_{11}}a_1,$$

$$d_3=\frac{\left(\frac{\rho h\omega^2}{C}-k_{12}^2\right)\left[\left(\frac{\rho h\omega^2}{C}-k_{11}^2\right)\cos(k_{11}a)+\left(k_{11}^2-\frac{\rho h\omega^2}{C}\right)\cos(k_{12}a)\right]}{\left(\frac{\rho h\omega^2}{C}-k_{12}^2\right)\sin(k_{12}a)k_{12}-k_{11}\left(\frac{\rho h\omega^2}{C}-k_{11}^2\right)\sin(k_{11}a)}a_1,\quad d_4=-\frac{k_{11}}{k_{12}}d_2,$$

where a_1 can be determined by orthogonality of mode shapes of free–free Timoshenko beam.

The coefficients satisfying the boundary conditions along y direction are given by

$$b_2 = -\frac{k_1\left[\left(k_1^2-\frac{\rho h\omega^2}{C}\right)\cos(k_1 b)-\left(k_2^2-\frac{\rho h\omega^2}{C}\right)\cos(k_2 b)\right]}{\left(k_1^2-\frac{\rho h}{C}\omega^2\right)[k_1\sin(k_1 b)-k_2\sin(k_2 b)]}b_1, \quad b_3=-b_1,$$

$$b_4 = \frac{k_2\left[\left(k_1^2-\frac{\rho h\omega^2}{C}\right)\cos(k_1 b)-\left(k_2^2-\frac{\rho h\omega^2}{C}\right)\cos(k_2 b)\right]}{\left(k_2^2-\frac{\rho h\omega^2}{C}\right)[k_1\sin(k_1 b)-k_2\sin(k_2 b)]}b_1,$$

$$c_1 = -\frac{\left(k_1^2-\frac{\rho h\omega^2}{C}\right)\cos(k_1 b)-\left(k_2^2-\frac{\rho h\omega^2}{C}\right)\cos(k_2 b)}{k_1\sin(k_1 b)-k_2\sin(k_2 b)}b_1, \quad c_2=-\frac{1}{k_1}\left(k_1^2-\frac{\rho h\omega^2}{C}\right)b_1,$$

$$c_3 = \frac{\left(k_1^2-\frac{\rho h\omega^2}{C}\right)\cos(k_1 b)-\left(k_2^2-\frac{\rho h\omega^2}{C}\right)\cos(k_2 b)}{k_1\sin(k_1 b)-k_2\sin(k_2 b)}b_1, \quad c_4=\frac{k_2^2-\frac{\rho h\omega^2}{C}}{k_2}b_1,$$

where b_1 can be determined by orthogonality of mode shapes of clamped–free Timoshenko beam.

References

[1] X.R. Ma, X.Y. Gou, T.S. Li, B.L. Wang, Development generalization of spacecraft dynamics, *Journal of Astronautics* 21 (2000) 1–5 (in Chinese).

[2] V.F. Krotov, A.B. Kurzhanski, National achievements in control theory the aerospace perspective, *Annual Reviews in Control* 29 (2005) 13–31.

[3] E.F. Crawley, J. de Luis, Use of piezoelectric actuators as elements of intelligent structures, *AIAA Journal* 25 (1987) 1373–1385.

[4] S.S. Na, L. Librescu, Optimal vibration control of thin-walled anisotropic cantilevers exposed to blast loadings, *Journal of Guidance, Control, and Dynamics* 23 (2000) 491–500.

[5] M.O.M. Carvalho, M. Zindeluk, Active control of waves in a Timoshenko beam, *International Journal of Solids and Structures* 38 (2001) 1749–1764.

[6] L. Librescu, O. Song, *Composite Thin-Walled Beams: Theory and Application*, Springer, Berlin, 2005.

[7] C. Mei, B.R. Mace, R.W. Jones, Hybrid wave/mode active vibration control, *Journal of Sound and Vibration* 247 (2001) 765–784.

[8] C.R. Fuller, G.P. Gibbs, R.J. Silcox, Simultaneous active control of flexural and extensional waves in beams, *Journal of Intelligence, Material, System and Structure* 1 (1990) 235–247.

[9] D.A. Wang, Y.M. Huang, Modal space vibration control of a beam by using the feedforward and feedback control loop, *International Journal of Mechanical Sciences* 44 (2002) 1–19.

[10] H.M. EL-Khatib, B.R. Mace, M.J. Brennan, Suppression of bending waves in a beam using a tuned vibration absorber, *Journal of Sound and Vibration* 288 (2005) 1157–1175.

[11] X. Pan, C.H. Hansen, Active control of vibratory power transmission along a semi-infinite plate, *Journal of Sound and Vibration* 184 (1995) 585–610.

[12] Z.K. Kusculuoglu, T.J. Royston, Finite element formulation of composite plates with piezoceramic layers for optimal vibration control applications, *Smart Materials and Structures* 14 (2005) 1139–1153.

[13] R.D. Mindlin, Influence of rotatory inertia and shear on flexural motions of isotropic, elastic plates, *ASME Journal of Applied Mechanics* 18 (1951) 31–38.

[14] D.J. Dawe, Finite strip models for vibration of Mindlin plates, *Journal of Sound and Vibration* 59 (1978) 441–452.

[15] D.J. Dawe, O.L. Roufaeil, Rayleigh–Ritz vibration analysis of Mindlin plates, *Journal of Sound and Vibration* 69 (1980) 345–359.

[16] A.W. Leissa, The free vibration of rectangular plates, *Journal of Sound and Vibration* 31 (1973) 257–293.

[17] C. Hu, T. Chen, W.H. Huang, Active vibration control of Timoshenko beam based on hybrid wave/mode method, *Acta Aeronautica et Astronautica Sinica* 28 (2007) 301–308.

[18] B.R. Mace, Wave reflection and transmission in beams, *Journal of Sound and Vibration* 197 (1984) 237–246.